The Australian Sounding Rockets Long Tom and Aeolus

by

D. A. H. BIRD, B.Sc., D.L.C., A.F.R.Ae.S.

(Flight Projects Group, Weapons Research Establishment, South Australia)

1. Introduction

The advent of the Skylark firings and the more recent trials of ballistic missiles such as the Black Knight firings, have demanded a continuous development of both ground and airborne instrumentation at Woomera Range; this in turn has raised the need for sighter rockets and instrumentation test vehicles with altitude capabilities in the 200,000-500,000 ft. range.

The need is currently being met by the rocket vehicles Long Tom and Aeolus. These rockets are of interest because they represent the first designed and built at W.R.E. that can be classed as high altitude rockets; also, they make possible the provision of relatively cheap and readily available vehicles for upper atmosphere research.

Aeolus has already been used in conjunction with the University of Adelaide in connection with a programme for the study of high altitude winds, and Long Tom has carried equipment to measure the frequency of incidence of meteoritic dust at altitudes above 200,000 ft. This latter experiment was made in conjunction with the Australian National University.

The first part of this paper contains a general description of Long Tom and Aeolus, followed by a summary of their respective performances. The second part contains a discussion of some of the design aspects of Long Tom. These apply in the main also to Aeolus.

2. General Description

2.1. LONG TOM

Long Tom is a two-stage rocket powered by four solid fuel Mayfly motors; these motors were designed and developed at the Rocket Propulsion Establishment, Westcott, and are the only major items that are "bought out". The general layout and leading dimensions are shown in Fig. 1.

The first stage consists of three Mayfly motors mounted "in parallel". The motors are located at their heads by an aluminium alloy casting and by a cast aluminium alloy spider just forward of the fin root leading edges. Some degree of fairing is provided by 18 SWG aluminium alloy sheet, as shown in Fig. 1. The rear fairing allows maximum advantage to be gained from the favourable body-fin lift interaction. The cast magnesium alloy fins are bolted directly to mild steel flanges welded to the motor venturis.

The second stage consists of a single Mayfly motor. This motor is mated to the first stage by means of a small cone on the nose of the boost head casting which picks up in the throat of the second stage venturi, as shown in Fig. 2. Separation at the end of burning of the first stage motors is effected by the differential drag of the two stages; an acceleration differential of the order of $9g$ ensures clean separation. Provision for instrumentation is made in the cylindrical compartment forward of the motor. This compartment is 9·2 in. in diameter and 35 in. long. Space for instrumentation or ballast is also available in the cast aluminium alloy nose cone, of semi vertex angle 7·5°. The cylindrical compartment can be subdivided anywhere along its length by pressure-tight bulkheads to provide a forward compartment sealed at ground level pressure, and a rear compartment vented to atmosphere. Three equi-spaced dural plate fins are mounted directly over the motor venturi on mild steel platforms welded to the venturi. These fins have steel leading edges notched into the dural plate to alleviate aerodynamic heating and erosion and to raise the critical flutter speed.

The all-up weight of the first stage is 1,400 lb.; the weight of the second stage varies between 520 lb. and 700 lb. depending on the instrumentation carried, giving a range of total weight at launch between 1,920 lb. and 2,100 lb.

2.2. AEOLUS

Aeolus is essentially a Long Tom second-stage rocket boosted by seven 5 in. light alloy plastic star motors in the first stage. The boost motor cluster is held at the rear by a light metal fairing, which also serves as a base for the four rectangular fins, and at the front by an aluminium alloy nose casting which is faired down to the diameter of the second stage. Mating of the two stages is again achieved by means of a small cone on the front of the boost nose casting which picks up in the venturi of the second stage. The boost assembly is shown in Fig. 3 and is of 16 in. diameter and 67 in. long. The all-up weight of the first stage is 600 lb. The weight of the second stage varies between 520 lb. and 650 lb., giving a range of weight at launch between 1,120 lb. and 1,250 lb. Long Tom and Aeolus are shown together, for comparison, in Fig. 4.

3. Payload

Payload can be carried in the cylindrical instrument compartment and also in the nose cone. The type and extent of instrumentation carried depends on the nature

Received 25th February 1960

Downloaded from https://www.cambridge.org/core. The Librarian-Seeley Historical Library, on 31 Mar 2017 at 17:38:00, subject to the Cambridge Core terms of use, available at https://www.cambridge.org/core/terms. https://doi.org/10.1017/S0368393100072667

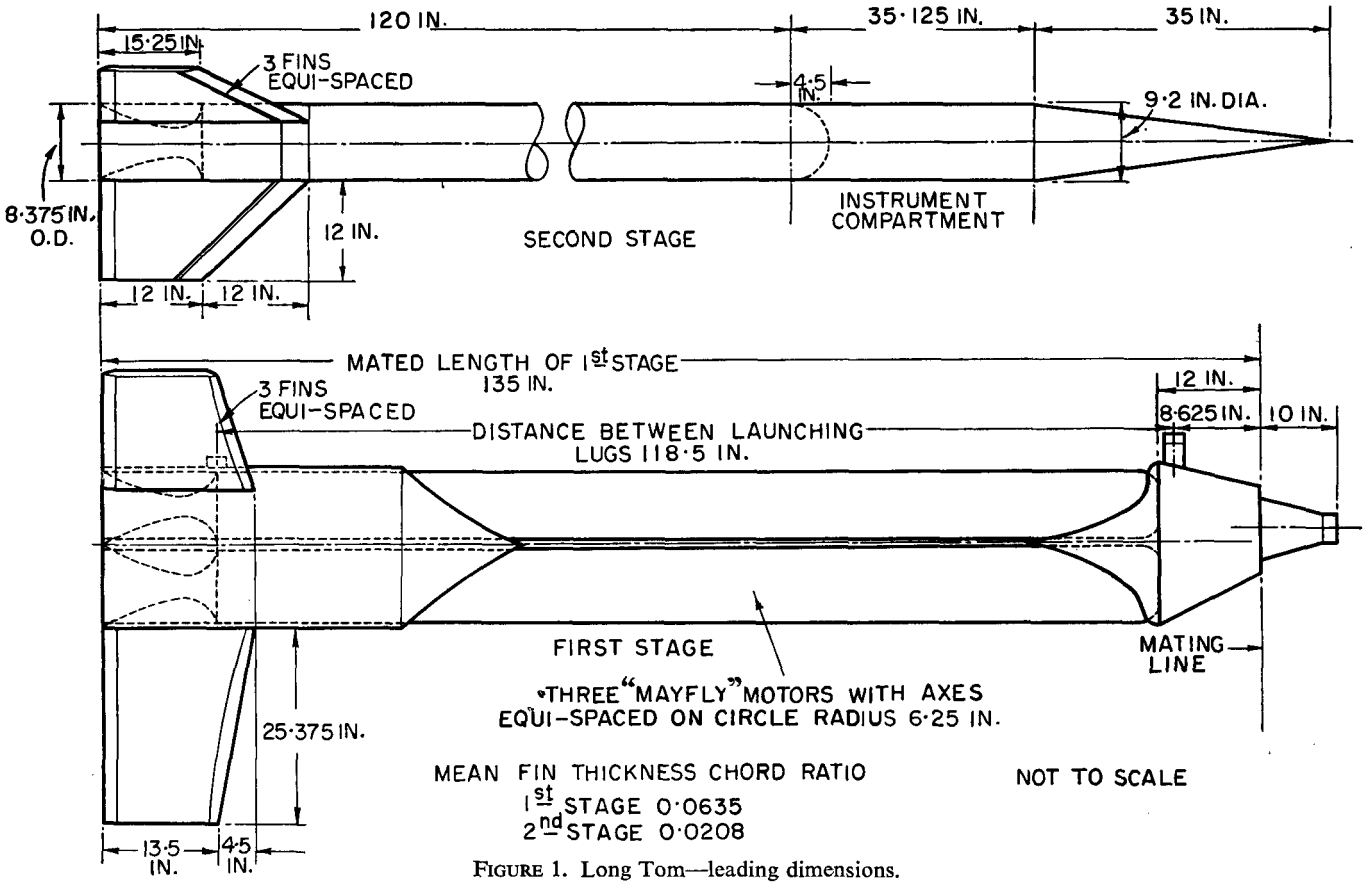

FIGURE 1. Long Tom—leading dimensions.

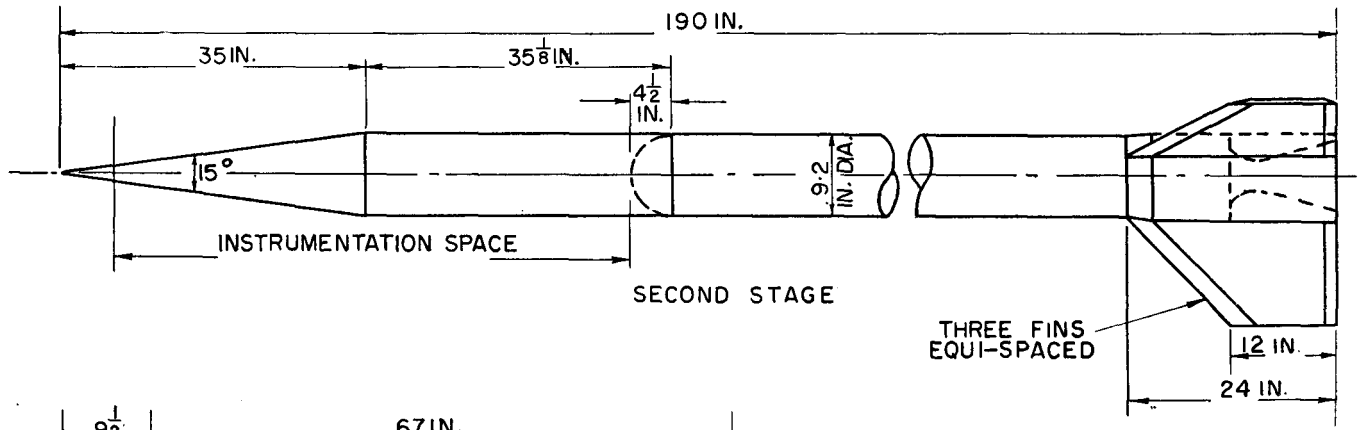

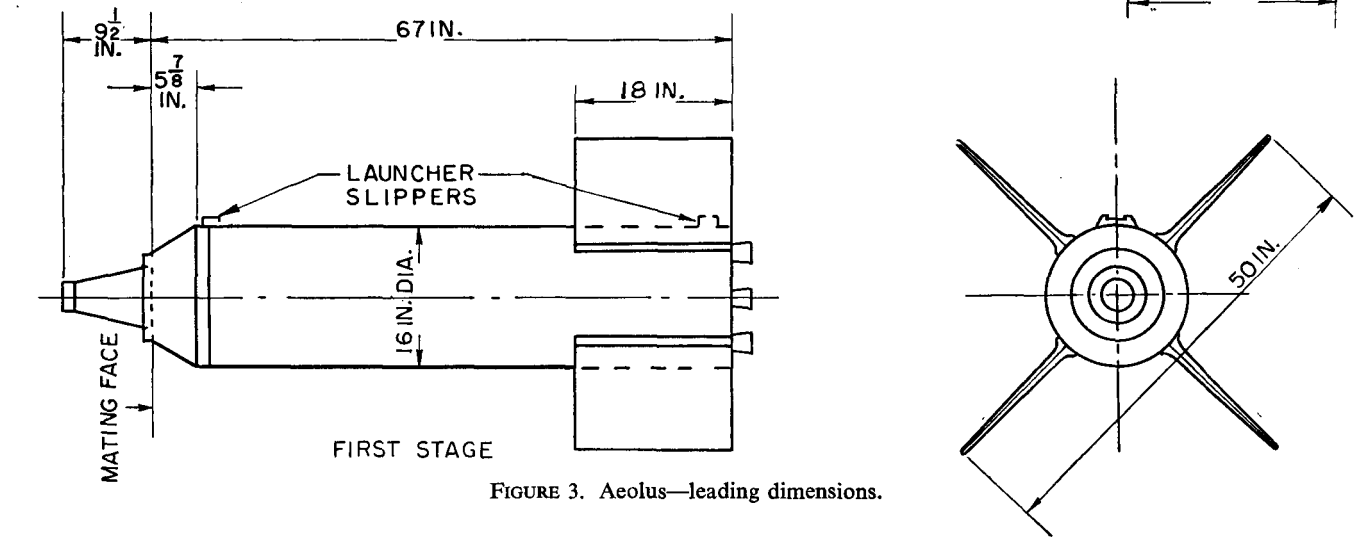

FIGURE 3. Aeolus—leading dimensions.

Downloaded from https://www.cambridge.org/core. The Librarian-Seeley Historical Library, on 31 Mar 2017 at 17:38:00, subject to the Cambridge Core terms of use, available at https://www.cambridge.org/core/terms. https://doi.org/10.1017/S0368393100072667

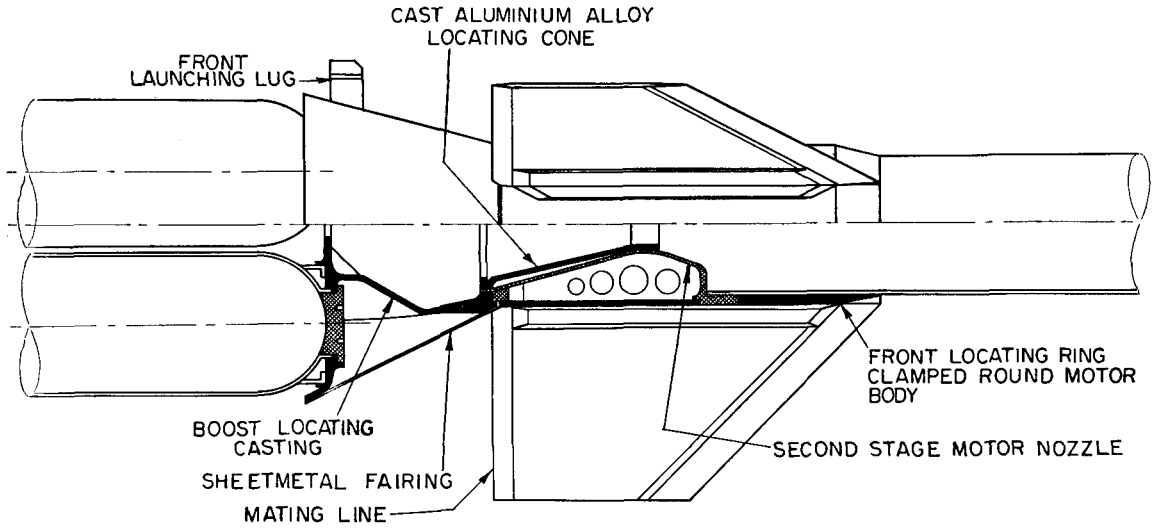

FIGURE 2. Long Tom—mating of first and second stage.

of the trial. The methods employed at Woomera Range to collect trials data have been described by Boswell[1] and will only receive brief mention here. When used in its prime role as a sighter rocket the minimum data required from Long Tom are time histories of its altitude, velocity and range, and for this purpose a W.R.E. multi-station radio tracking beacon (MTS unit) is carried as standard equipment. Also standard are the firing circuit clocks and batteries for ignition of the second stage motor. After inclusion of the MTS unit, firing clocks and batteries, some 1,950 cu. in. of space are still available in the instrument compartment and nose cone. In other cases data are required that can only be measured on, or in, the round itself, in which case a sub-miniature 24-channel time multiplexed FM/AM telemetry system[1] is used. Fig. 5 shows a typical installation in the nose cone of Long Tom. In this system the physical quantity to be measured is transformed into an e.m.f. or an inductance and fed into the modulator. In the modulator the quantity is transformed into a sub-carrier frequency which is used to amplitude-modulate the RF oscillator output. The system can handle 24 information channels by means of a mechanical switch which rotates at rates up to 120 revs./sec.

Individual channels can be sub-commutated if required. Sub-carrier frequencies are in the band 130-160 kc./sec., while the carrier frequency is in the band 435-490 Mc./sec.

From performance considerations the maximum allowable weight of the second stage, in the case of Long Tom, is 700 lb., allowing the carriage of 180 lb. of payload if this can fit the space available. Aeolus, with its less powerful boosting stage, is limited to a maximum payload of 130 lb.

Normally the instrument head of either vehicle does not separate from the motor after burning. Impact velocities are high, being of the order of 4,000 ft./sec. The rounds are completely destroyed by the force of impact. However, if recovery of any instrumentation is desired, the head can be explosively separated from the

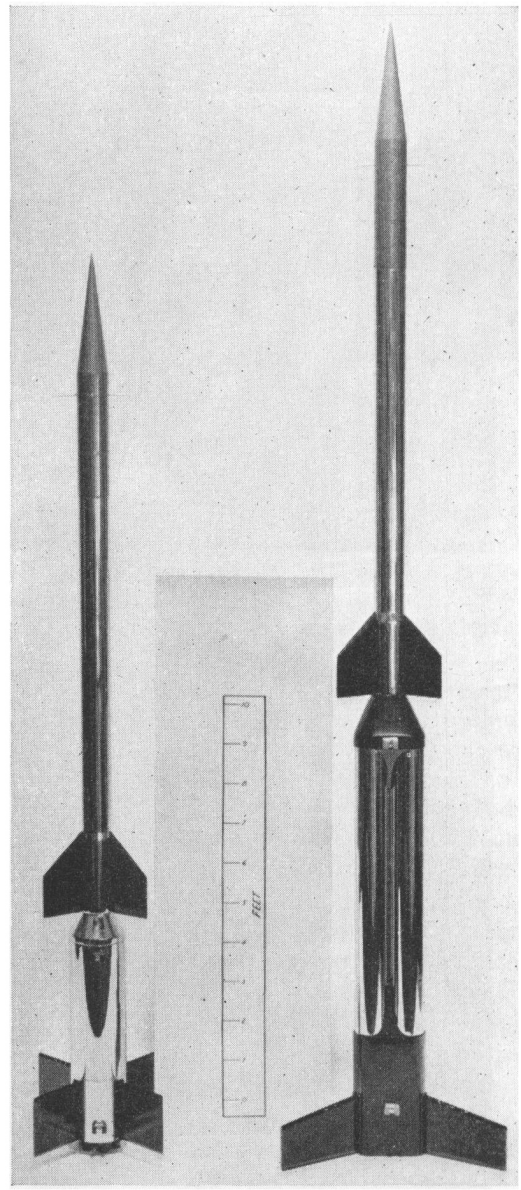

Aeolus. Long Tom.

FIGURE 4.

Downloaded from https://www.cambridge.org/core. The Librarian-Seeley Historical Library, on 31 Mar 2017 at 17:38:00, subject to the Cambridge Core terms of use, available at https://www.cambridge.org/core/terms. https://doi.org/10.1017/S0368393100072667

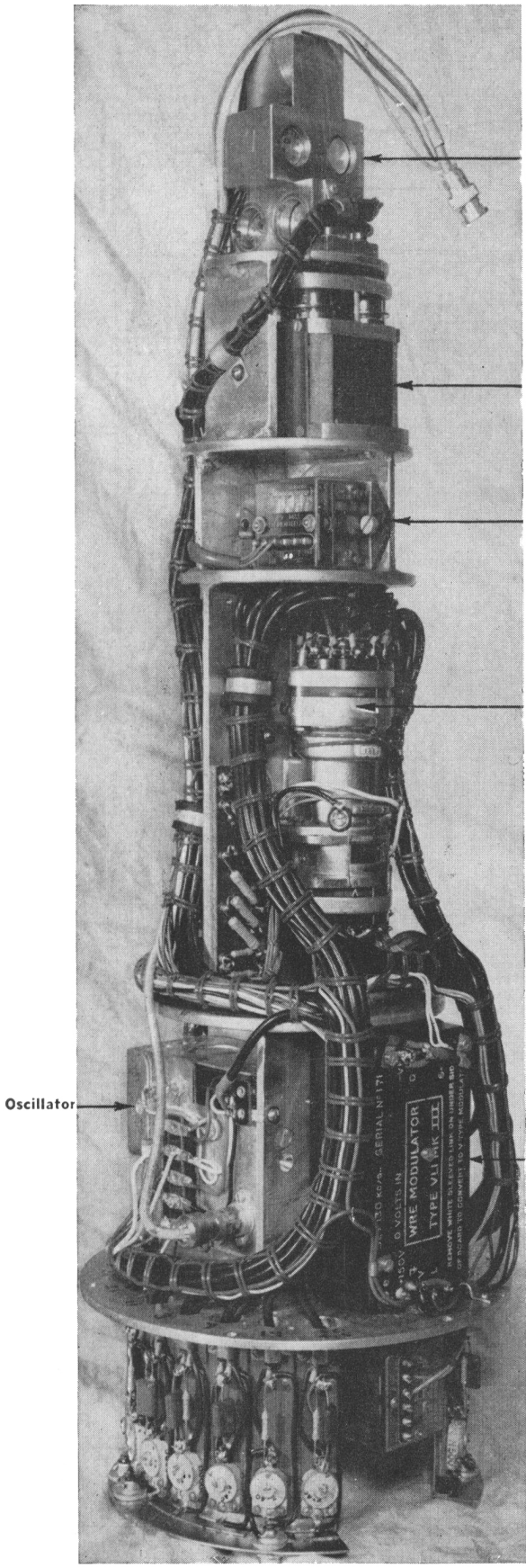

FIGURE 5. Installation of telemetry equipment in nose cone.

motor and brought to earth by parachute. A high degree of control can be exercised over the location of the explosive separation by the use of cordtex cutting charge. A special ring is inserted in the body at the point of required separation, just aft of the parachute compartment, and the cordtex charge is laid in a groove machined round the circumference of the ring. The outer skin of the round fits over the groove and the cordtex. The charge is detonated electrically at the appropriate time by a timing switch and produces a clean circumferential cut in the skin. The weight of the recovery system is about 12 lb., which must, of course, be subtracted from the useful payload.

With Aeolus, separation of the head occurs in the region of 150,000 ft. to 200,000 ft. when the round has a velocity in the region of 2,000 to 3,000 ft./sec. It has been found possible to deploy successfully a parachute at these altitudes and to obtain an adequate shock-free deceleration of the head without the use of a drogue; impact velocities are reduced to the order of 50 ft./sec. Fig. 6 shows the head of an Aeolus vehicle after recovery by a parachute released at 200,000 ft. In the one case where parachute recovery has been attempted with Long Tom, a nylon parachute released at 300,000 ft. failed to decelerate the head, which had an impact velocity of 400 ft./sec. (the terminal velocity of the head). On examination of the wreckage the parachute was found to be in a fused condition, indicating severe heating effects. The velocity of Long Tom at the time the parachute was deployed was approximately 3,000 ft./sec.

It is not possible to draw any firm conclusions on the limited evidence available, but it would seem that the successful deployment of a parachute at the altitudes in question must be sensitive to altitude, or velocity or both.

Probably the easiest way to ensure that the parachute is successfully deployed is to break up the round at high altitude and allow its unstable tumbling motion to persist to low altitude, say 20,000 ft., where the head has decelerated to its terminal velocity and the parachute may be safely deployed.

4. Launching

The same launcher, with slight modifications to the launching rails, can be used for both Long Tom and Aeolus. The launcher is of tubular steel construction and consists of a boxed beam pivoted near its mid point for training in elevation. The beam and its supporting structure are mounted on castors running in a circular track set in the concrete launching pad, thus allowing rotation of the launcher through 360° in azimuth. The Long Tom boost body is suspended by fore and aft lugs from two I-section rails of equal length mounted below the launcher beam. The lugs clear their separate rails simultaneously, thus minimising tip-off effects. The lugs on the Long Tom boost body are approximately 10 ft. apart, giving an effective launcher length of 10 ft. A launcher length of 10 ft. would result in Aeolus, with its less powerful boost stage, leaving the launcher with

Downloaded from https://www.cambridge.org/core. The Librarian-Seeley Historical Library, on 31 Mar 2017 at 17:38:00, subject to the Cambridge Core terms of use, available at https://www.cambridge.org/core/terms. https://doi.org/10.1017/S0368393100072667

rather low velocity, so the two rails are replaced by a single rail 23 ft. long.

Long Tom mounted on the launcher is shown in Fig. 7.

5. Performance

The trajectories followed by Long Tom and Aeolus are identical in sequence and may be divided into five separate phases:—

(*i*) The launching phase, starting with the ignition of the first-stage motors and ending when the combined stages clear the launching rail.

(*ii*) The first thrusting or boost phase, ending when the first-stage motors have finished burning and are jettisoned.

(*iii*) Coasting of the second stage before ignition of its motor.

(*iv*) The second thrusting phase, starting with the ignition of the second-stage motor.

(*v*) The final coasting phase of the second stage after motor burnout.

Only phases (*ii*) to (*v*), the flight phases, will be considered here.



FIGURE 6. Head of Aeolus after recovery by parachute from 200,000 ft.

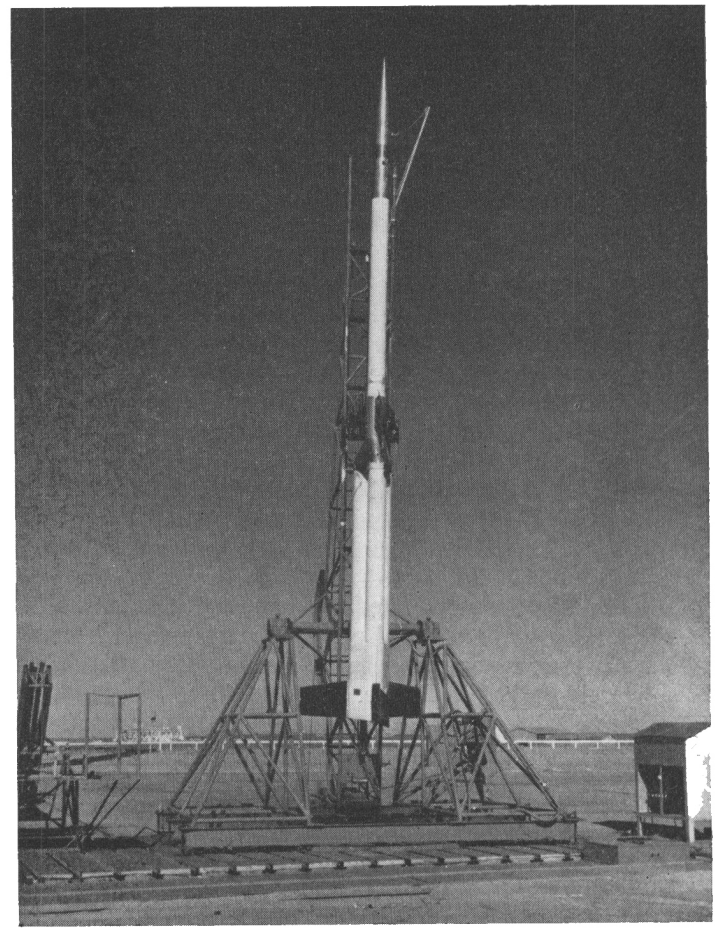

FIGURE 7. Long Tom mounted on the launcher.

5.1. LONG TOM

At the end of phase (*ii*), first burning, Long Tom reaches a velocity of the order of 3,000 ft./sec. at an altitude of about 7,000 ft. The duration of this phase is between 4 and 5 seconds and is immediately followed by the separation of the two stages under differential drag action.

A number of factors govern the choice of time of ignition of the second-stage motor, and the optimum duration of phase (*iii*) for maximum peak altitude with an upper Mach number limit of 6 has been found to be between 15 and 20 seconds after launch. At the end of phase (*iii*) the round has decelerated to approximately 1,700 ft./sec. and has reached an altitude in the region of 40,000 ft.

During phase (*iv*), the burning period of the second-stage motor, the round accelerates to its peak velocity of approximately 500 ft./sec. at an altitude of 50,000 ft.

After the second-stage motor has finished burning the rocket coasts on until impact, passing though a peak altitude of between 300,000 ft. and 600,000 ft., depending on its weight and angle of launch.

The ground range covered depends on the weight of the second stage and the angle of launch, and is discussed more fully in Part 2. For typical firings the range is between 80 and 100 miles.

Downloaded from https://www.cambridge.org/core. The Librarian-Seeley Historical Library, on 31 Mar 2017 at 17:38:00, subject to the Cambridge Core terms of use, available at https://www.cambridge.org/core/terms. https://doi.org/10.1017/S0368393100072667

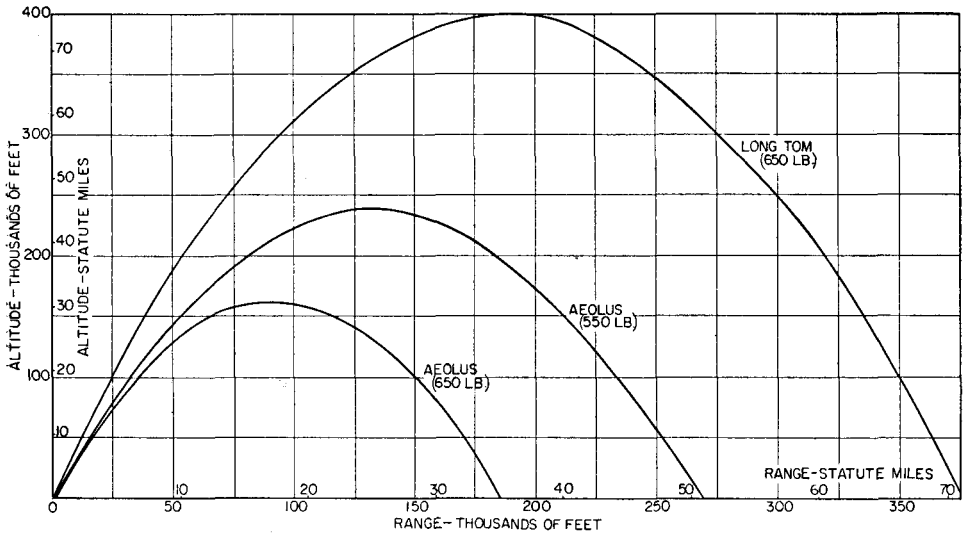

FIGURE 8. Typical trajectories for Long Tom and Aeolus, launched at 80° elevation.

5.2. AEOLUS

The boost motors fitted to Aeolus give about half the total impulse of the Long Tom boost stage, hence the performance is somewhat reduced. Aeolus reaches a velocity of 1,500 ft./sec. at 3,000 ft. at the end of phase (*ii*). The second-stage motor ignites 16 sec. after launch when the velocity is 850 ft./sec. and the altitude between 16,000 and 17,000 ft. The peak velocity at the end of second burning is of the order of 4,000 ft./sec. at 24,000 ft. Peak altitudes are in the range of 160,000 to 300,000 ft.

Typical trajectories for Long Tom and Aeolus are compared in Fig. 8. The Long Tom trajectory is for a second stage weight of 650 lb. and a launch elevation of 80°. This weight represents a useful payload of 130 lb. and the peak altitude achieved is of the order of 400,000 ft., with a range in the region of 70 miles. Aeolus, when launched at the same elevation, can carry 130 lb. payload to 165,000 ft., or 30 lb. payload (total second stage weight 550 lb.) to 240,000 ft., the ranges being 35 miles and 50 miles respectively.

PART II—THE DESIGN OF LONG TOM

NOTATION

C_D	drag coefficient
C_{D_B}	base drag coefficient
C_f	skin friction coefficient
D_B	base diameter
D_N	jet nozzle exit diameter
$\frac{dC_n}{d\alpha}$	slope of normal force curve
H_j	jet total pressure
M	Mach number
p_j	static pressure at jet exit
p_∞	static pressure of free stream
R	Reynolds number
$X_{c.p.}$	distance of resultant c.p. aft of tip of nose cone
$x_{c.p.}$	distance of c.p. (of component) aft of tip of nose cone
γ	ratio of specific heats for air

1. Choice of Propulsion Unit

The prime objective of the Long Tom design was to provide an unguided sighter rocket that was simple, could be readily prepared and would reliably achieve a performance in the 300,000 to 500,000 ft. altitude bracket with about 100 lb. payload.

To be operationally acceptable the firing of this sighter should not be unduly restricted by adverse weather conditions. The simplicity should also extend to the launching and ground testing facilities. From the consideration of simplicity a solid fuel propulsion system was decided upon from the outset. The decision then to be made was whether to have a single-stage long-burning motor, or two stages of the same total impulse as the single stage, but each of shorter duration.

If high velocities are attained during the early stages of flight while the missile is still at low altitude, the drag penalty becomes high and power is wasted overcoming this. Fig. 9 compares two possible trajectories of a hypothetical single-stage vehicle having a total impulse of 86,000 lb./sec. A launch weight of 700 lb. and all-burnt weight of 270 lb. were assumed and a representative drag function was included in the trajectory computations. From Fig. 9(*a*), if the motor is allowed to burn for 3 sec. with an average thrust of 30,000 lb., curve (*a*), the altitude reached is 180,000 ft. When the motor burning time is extended to 15 sec. with an average thrust of 6,000 lb., the peak altitude increases to 250,000 ft. (curve (*b*)). Fig. 9(*b*) shows the velocity-height relationship for these two cases. With the short-burning motor the rocket reaches a peak velocity of 5,250 ft./sec. at 8,000 ft., the drag at this point being 3,400 lb. and the maximum acceleration during burning being 76*g*. With the long-burning motor the rocket takes 32,000 ft. to reach a peak velocity of 4,500 ft./sec., when the drag is 1,300 lb. The peak acceleration during thrusting is 13·5*g*.

From these results it would appear desirable to keep the mean thrust level down so that the rocket has a relatively low acceleration, spread over a long burning time. However, this has its disadvantages for an unguided ballistic rocket. A rocket with axial thrust is particularly susceptible to deviation of the trajectory due to wind effects during its thrusting period, so that if

Downloaded from https://www.cambridge.org/core. The Librarian-Seeley Historical Library, on 31 Mar 2017 at 17:38:00, subject to the Cambridge Core terms of use, available at https://www.cambridge.org/core/terms. https://doi.org/10.1017/S0368393100072667

the velocity off the end of the launcher and subsequent accelerations are too low, the problem of estimating and correcting for winds varying both in speed and direction over a considerable height range becomes rather severe. One is then faced with the choice of laying down restrictions on permissible meteorological conditions for firing or, of making an extremely long and cumbersome launcher to ensure an adequate velocity when the rocket becomes airborne. Both these vitiate the objectives which the rocket was designed to attain.

The foregoing example assumes that in both cases the total impulse is employed in a single-stage continuous-burning motor, the carcase of which is retained throughout the flight. By using two stages, the drag penalty incurred by the single short-burning stage can, to some extent, be overcome while the advantages of high launch acceleration are retained. The first stage is jettisoned immediately it has finished burning, thus reducing the drag and the dead load to be carried.

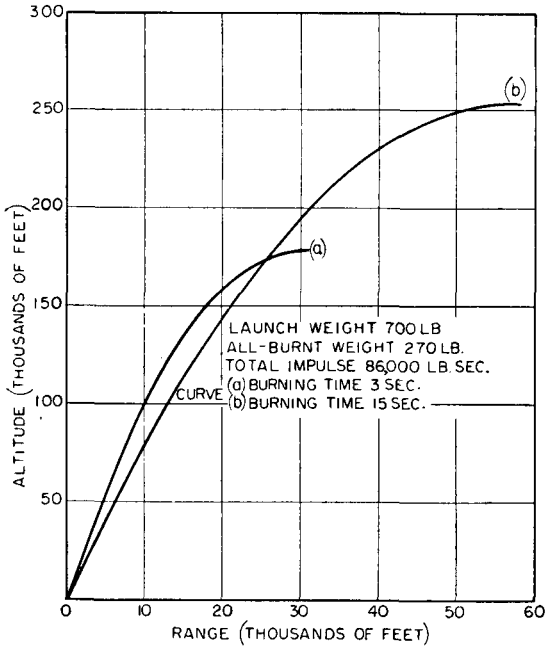

(*a*) Altitude as a function of range.

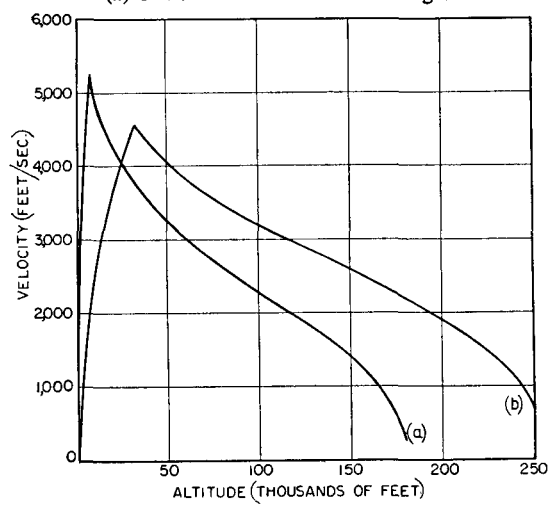

(*b*) Velocity as a function of altitude.

FIGURE 9. Effect of burning time on performance.

In general, maximum peak altitude will be reached if the second-stage motor is ignited immediately; however, this would result in an excessively high peak velocity at a relatively low altitude, with consequent excessive dynamic pressures and skin temperatures. In fact, ignition of the second-stage motor can usually be delayed for a fairly long period before the peak altitude is significantly reduced, but the peak velocity is reduced and occurs at a higher altitude. Long Tom coasts for 20 seconds before the second-stage motor is ignited and 25,000 ft. are gained during this coasting period. The second-stage motor is then ignited and the rocket is allowed to coast on after burning without separation from the head. At the end of second burning the rocket has reached an altitude between 50,000 ft. and 60,000 ft. and has a velocity of the order of 5,000 ft./sec. At these altitudes the air density is low and the high velocities achieved by the short-burning high thrust motor do not impose such a high drag penalty as at the end of the first burning period. In fact, in the second burning stage the long-burning motor shows little gain over the short-burning one from the altitude performance point of view. This two-stage technique is about as efficient as having one long-burning non-separating motor when considered in terms of useful payload and, because the range of solid fuel motors available at the time favoured it, this was the technique adopted for Long Tom. These remarks apply only to rockets of performance capabilities similar to Long Tom and do not necessarily hold for the problem of optimum thrust programming in general.

It is interesting to compare Long Tom with the upper atmosphere research rocket Skylark[2] which has a single long-burning motor and is non-separating. The useful payload is of the same order—150 lb. for Skylark, 130 lb. for Long Tom. Skylark is fired from a launcher some 100 ft. in length; Long Tom employs a 10 ft. launcher, yet the wind dispersion problem with Long Tom is slightly less severe than with Skylark. The Skylark total impulse is roughly twice that of Long Tom and yet the peak altitudes achieved are comparable, about 500,000 ft. for Skylark, 400,000 ft. for Long Tom. Although the useful payloads are of the same order, Skylark actually lifts a total dead weight of 800 lb. to 500,000 ft., while Long Tom lifts only 400 lb. to 400,000 ft.

The significant factor is that Skylark was designed to lift its payload, which consists of a wide variety of research apparatus, into the upper atmosphere without subjecting it to very high acceleration. Skylark does not exceed an acceleration of 9*g* at any stage of its ascent, whereas with Aeolus and Long Tom the type of apparatus carried as payload must be able to withstand accelerations as high as 50*g*.

As has already been mentioned, an increase in the burning time of the second stage without change in the total impulse would not improve the altitude performance overmuch, since the drag penalty incurred by high velocities is much reduced at the altitudes where the peak velocity is reached (60,000 ft.). An increase in burning time of the boost stage with a reduction in the mean thrust, acceleration and peak velocity, would

Downloaded from https://www.cambridge.org/core. The Librarian-Seeley Historical Library, on 31 Mar 2017 at 17:38:00, subject to the Cambridge Core terms of use, available at https://www.cambridge.org/core/terms. https://doi.org/10.1017/S0368393100072667

certainly result in a significant gain in altitude; but, from the point of view of wind deviation reasonably high launch velocities (and therefore accelerations) are desirable if a short launcher length is desired. The answer lies in shaping the thrust characteristic to give a high acceleration during the launch phase and a reduced thrust over an extended burning time for the remainder of the thrusting phase. Modern techniques in solid fuel motor design render this type of thrust shaping a possibility, which will almost certainly be attempted in some future version of Long Tom.

2. Drag

Having decided on the propulsion unit, a preliminary layout of the two stages can be made and an approximate calculation of the weight and centre of gravity can be carried out for the various flight stages. Before stability estimates can be made a knowledge of the trajectory is required and to compute this, the drag coefficient C_D as a function of Mach number and altitude must be computed. All normal force and drag coefficients are referred to the body cross-sectional area of 0·462 ft.^{2}

During the first thrusting phase, when the two stages are combined, supersonic velocities up to a Mach number of 3 are achieved at altitudes of some 6,000 ft. Drag forces are only a small proportion of the thrust and need only be known approximately. After separation of the stages, particularly in the first coasting phase, drag must be estimated as accurately as possible if any reliable trajectory computations are to be made.

Drag forces are normally divided into drag at zero incidence and induced drag, or drag due to lift. Since in the performance studies carried out at this stage the round is assumed to follow a ballistic trajectory, only zero incidence drag forces need be estimated. These are further divided into profile drag or wave drag, skin friction and base drag.

Wave drag arises from the shock pattern at the nose of the body, the shock patterns at the fin leading edges and from the shocks arising at any surface discontinuity, such as fin-body junctions or any discontinuous increase in body contour slope. Both Long Tom and Aeolus have a conical nose of 7·5° semi-vertex angle, fitted to a cylindrical afterbody. The wave drag of cones can be derived from the data computed by Kopal[3].

Both the first and second stage fins are of parallel-double wedge section and their contribution to the wave drag can be computed from the charts prepared by Bishop and Cane[4].

The effect of Reynolds number on body skin friction is given in the case of a turbulent boundary layer under zero heat transfer conditions by the semi-empirical formula[5] for the mean skin friction coefficient C_f:—

$$C_f = 0{\cdot}074R^{-1/5}\left(1+0{\cdot}9\frac{\gamma-1}{2}M^2\right)^{-2{\cdot}2/5}$$

where R = Reynolds number based on overall body length l.
γ = ratio of specific heats for air.
M = free stream Mach number.

The results given by this formula are similar to those given by other semi-empirical formulae.

Perhaps the most difficult drag effect to estimate with any accuracy is the base drag both with motor off and during thrusting. Many factors affect the pressure on the blunt base of a body—such as body shape, presence of fins, boundary layer thickness and Reynolds number, although for a fully turbulent boundary layer this is small. The presence of a jet can also substantially alter the base pressure. Some useful work has recently been done by Love[6] in which he derives a semi-empirical method for determining base drag by drawing an analogy between the flow over a two-dimensional base and the peak pressure rise associated with boundary layer separation in flow over a two-dimensional forward facing step. The analogy is extended to bodies of revolution, and can be applied to cylindrical and boat-tailed bases in the Mach number range 1·0 to 8·0, although the experimental data used extend only to $M=4{\cdot}0$. It is shown that for a turbulent boundary layer Reynolds number effects are small. The effects of fins, fore-body and angle of attack are also covered.

An accurate quantitative method for determining base drag in the presence of a jet has yet to be found; however, Cortright[7] has shown how useful the peak pressure rise analogy can be in estimating trends of such effects as those due to jet separation and base diameter/nozzle diameter ratio.

Long Tom has a convergent-divergent nozzle of exit-to-throat area ratio of approximately 5. When such a nozzle is operating at its optimum design point, the static pressure at the nozzle exit p_j is equal to the free stream static pressure p_∞ and the base pressure would be much the same as in the motor-off case, but acting only over the annulus surrounding the jet exit. Hence the base drag would be reduced by a factor

$$\frac{\text{area of annulus}}{\text{total area of base}}.$$

The ratio of base pressure p_b to free stream static pressure p_∞ is a function both of jet static pressure ratio p_j/p_∞ and the ratio of base diameter D_B to nozzle diameter D_N. When $p_j/p_\infty=1$, as above, the convergent-divergent nozzle is fully expanded.

The chamber pressures in the Mayfly motors employed in both stages of Long Tom are such that at sea level p_j/p_∞ is of the order of 2 and in the region of 40,000 ft., when second ignition occurs p_j/p_∞ is of the order of 10; the nozzles are under-expanded during both burning phases.

Cortright[7] has calculated the ratio of base pressure p_b to free stream static pressure p_∞ as a function of jet static pressure ratio p_j/p_∞ and D_B/D_N. The configuration he considered was a convergent nozzle fitted in an afterbody with 5·6° boat-tail, operating at a Mach number of 1·9. Since the boat-tail angle and the free stream Mach number will affect the pressures in the external flow, this must affect the base pressure ratio for a given p_j/p_∞, hence Cortright's curves are not strictly applicable to Long Tom which has a cylindrical afterbody. The flow characteristics of the convergent nozzle

Downloaded from https://www.cambridge.org/core. The Librarian-Seeley Historical Library, on 31 Mar 2017 at 17:38:00, subject to the Cambridge Core terms of use, available at https://www.cambridge.org/core/terms. https://doi.org/10.1017/S0368393100072667

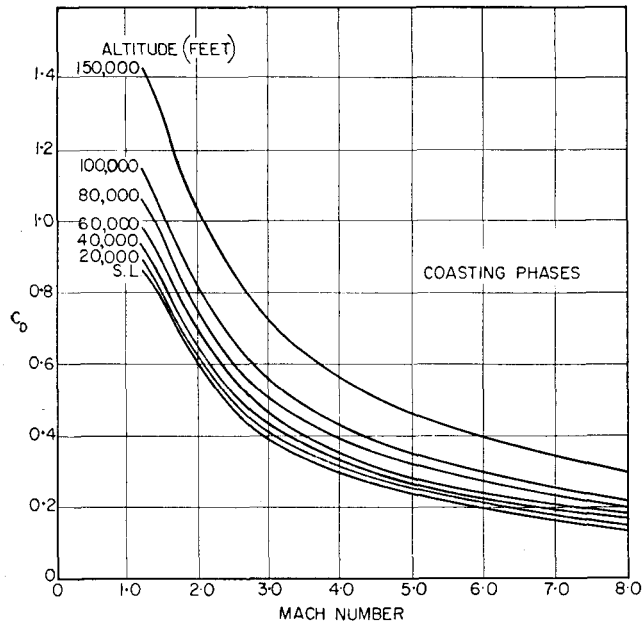

FIGURE 10. Long Tom and Aeolus drag coefficient for second-stage coasting.

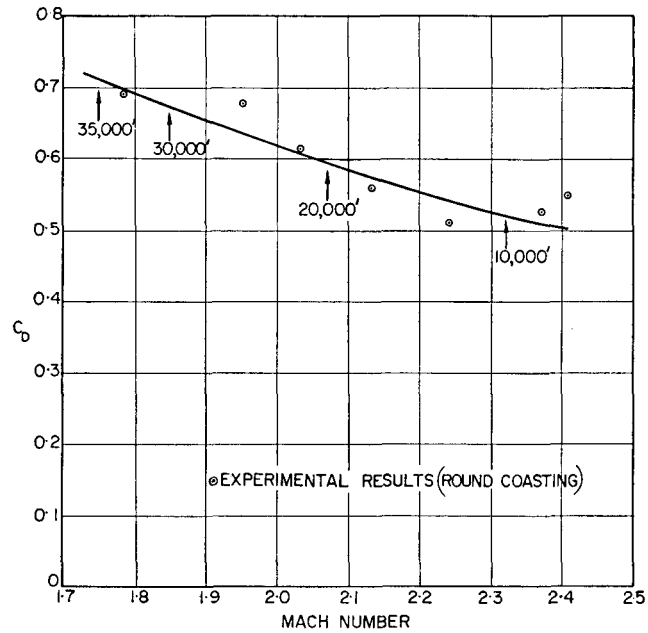

FIGURE 11. Comparison between drag estimates and trial results.

are also somewhat different from the convergent-divergent nozzle of Long Tom, but the effect of this is small. However, using these curves as a guide it was concluded that during first burning, when p_j/p_∞ is of the order of 2, the drag coefficient C_{D_B} (referred to body cross-sectional area) due to pressure on the base annulus would be about one quarter the value of C_{D_B} (referred to the same area) when the motor was not burning and the whole base area was contributing to base drag. During second burning the C_{D_B} with motor on would be sensibly zero.

In view of the fact that during burning the thrust is large compared with the drag, any base drag effects on this configuration would be swamped by uncertainties in thrust prediction, so base drag was taken as zero during both thrusting phases. In other cases, where jet exit diameter is small compared with base diameter, the base drag during thrusting can exceed the coasting value. The overall drag coefficient computed for the Long Tom second stage during coasting is shown as a function of Mach number and altitude in Fig. 10. These curves apply also to Aeolus. A check on the accuracy of these drag estimates was made after the initial firing of Long Tom. The experimental points in Fig. 11 were derived from the trajectory data; the full line was derived by using the theoretical curves of Fig. 10 in conjunction with height and Mach number data from the trial. The agreement shown between the experimental points and the estimated line in Fig. 11 is sufficiently good for general performance estimates.

3. Static Stability

Having obtained the likely Mach number range from the still-air performance estimates, it must be ascertained that the rocket has adequate static stability over all the flight phases. Static margin is here expressed as the distance the resultant centre of pressure (c.p.) lies behind the centre of gravity (c.g.). The criterion adopted is that for adequate static stability the static margin should not be less than 5 per cent of the body length. The initial position of the c.g. is a function of the initial weight of the round and, since the instrument compartment is at the forward end of the round, the c.g. is farthest aft when the round is in its condition of least loading. As the motor burns the c.g. moves forward some six inches. A lightly loaded round, of course, achieves a high Mach number and fin power deteriorates with increase in Mach number; the combination of high Mach number, lower fin power and aft c.g. position tends to make the low loading cases critical as far as static stability is concerned.

The c.p. position $X_{c.p.}$ of the fin-body combination is determined from the relation

$$X_{c.p.} = \frac{\left(\frac{dC_n}{d\alpha}\right)_{body}(x_{c.p.})_{body} + \left(\frac{dC_n}{d\alpha}\right)_{fins}(x_{c.p.})_{fins}}{\left(\frac{dC_n}{d\alpha}\right)_{body} + \left(\frac{dC_n}{d\alpha}\right)_{fins}}$$

where $\left(\frac{dC_n}{d\alpha}\right)_{body}$ is the slope of the normal force curve at zero incidence of the body alone.

$\left(\frac{dC_n}{d\alpha}\right)_{fins}$ is the slope of the normal force curve at zero incidence of the isolated fins, adjusted for fin body interference.

$(x_{c.p.})_{body}$ is the distance of c.p. of the body alone from the tip of the nose cone.

$(x_{c.p.})_{fins}$ is the distance of the fin c.p. from the tip of the nose cone adjusted for fin body interference.

The interference effects considered are the effective increase in fin normal force due to the upwash field created by the body at incidence, and the modification

Downloaded from https://www.cambridge.org/core. The Librarian-Seeley Historical Library, on 31 Mar 2017 at 17:38:00, subject to the Cambridge Core terms of use, available at https://www.cambridge.org/core/terms. https://doi.org/10.1017/S0368393100072667

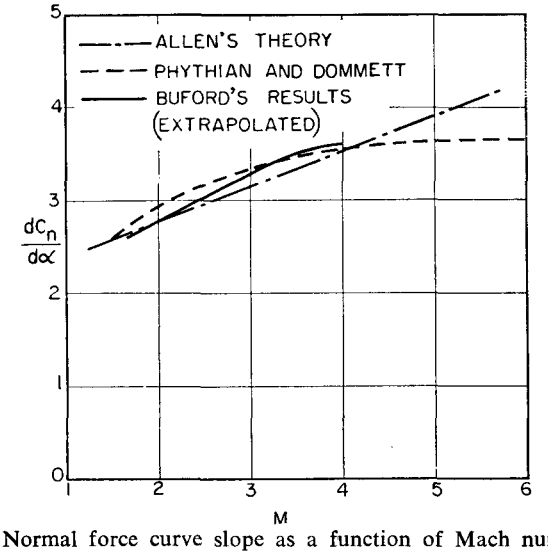

(*a*) Normal force curve slope as a function of Mach number.

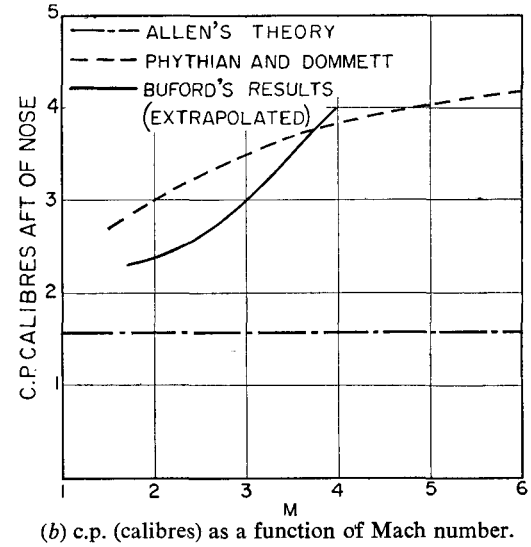

(*b*) c.p. (calibres) as a function of Mach number.

FIGURE 12. Normal force and centre of pressure of a 10° cone-cylinder. Overall fineness ratio 20, nose fineness ratio 2·8.

of body lift due to the Mach cones originating at the fin leading edge roots. Both these effects are combined as a factor on the isolated fin normal force curve slope and on the isolated fin c.p. position.

The method of allowing for fin-body effects follows closely that given by Pitts, Nielsen and Kaattari[8], although other methods are used for computing the lift curve slopes and c.p. positions of the isolated fins and bodies.

A semi-empirical method based on Allen's theory[9] had been used in estimating the body c.p. position at low supersonic Mach numbers but it was found that this failed to predict any rearward shift of body c.p. with increase in Mach number, and resulted in an undesirable restriction on the limit of permissible c.g. position and hence, on the minimum loading. Some recent work by Buford[10] indicated that the body normal force curve slope might be expected to decrease beyond a Mach number of about 3 or 4, accompanied by a slight rearward shift of the body c.p.; both these effects alleviate the stability problem at high Mach numbers. Slender body theory attributes no lifting effect to the cylindrical after-body of a cone cylinder at or near zero incidence, while calculations based on the shock expansion method of Syvertson and Dennis[11] indicate a lift carry-over effect round the shoulder of the cone cylinder. A review of current information has been made by Phythian and Dommett[12] who present semi-empirical curves enabling forces on cone cylinder combinations to be readily estimated at Mach numbers up to 6.

Buford's experimental results are confined to a nose semi-vertex angle of 10° and since cone angle is one of the most important parameters governing flow conditions at the shoulder, they are not readily applicable to other cases. The normal force curve slope and position for a 10° cone cylinder of fineness ratio 20 (approximating to Long Tom) were computed by the semi-empirical slender body theory and by the semi-empirical method of Phythian and Dommett. The results are compared with Buford's experimental results in Fig. 12. Buford's results extend only to a fineness ratio of 14 and it was necessary to extrapolate them somewhat. It will be seen in Fig. 12(*a*) that above a Mach number of 4 slender body theory would tend to over-estimate normal force curve slope. The agreement between Phythian and Dommett's method and Buford's experimental results is good. In the case of centre of pressure position, Fig. 12(*b*) shows that the constant c.p. given by slender body theory is too far forward over the whole Mach number range considered. The comparison between Phythian and Dommett's method and Buford's results is not so good as in the case of normal force curve slope, but the difference is not greater than 0·6 calibre at Mach numbers below 4. Beyond this, the trend of the experimental (Buford's) curve is still of positive slope while Phythian and Dommett's curve tends to flatten out at a lower value. At the lower Mach numbers fin power is sufficiently high to provide adequate stability even if slender body theory is used for the body, but as the hypersonic region is approached fin power decreases fairly rapidly and it is then that body lift becomes significant. Fig. 12(*b*) would indicate that Phythian and Dommett's method gives a conservative estimate of body c.p. in the higher Mach number range and is adequately consistent with experimental data in the lower supersonic range ($1 < M < 4$).

The method of Ref. 12 was used to re-compute the static margin of the Long Tom second stage both before and after motor burning. At the end of burning of the second stage, Mach numbers between 5 and 7 can be achieved, and this is the most critical flight phase from the point of view of stability. In Fig. 13 static margin as a percentage of body length is shown for the second stage as a function of Mach number and c.g. position, expressed in calibres aft of the nose (1 calibre $=9{\cdot}2$ in.). The approximate c.g. positions during the final coasting phase are shown by dotted lines for second stage initial weights of 500 lb., 550 lb., 600 lb. and 700 lb. Fig. 14 shows the peak Mach number attained for the range of second stage weights. For weights below 550 lb. approximately, the round is likely to have a static

Downloaded from https://www.cambridge.org/core. The Librarian-Seeley Historical Library, on 31 Mar 2017 at 17:38:00, subject to the Cambridge Core terms of use, available at https://www.cambridge.org/core/terms. https://doi.org/10.1017/S0368393100072667

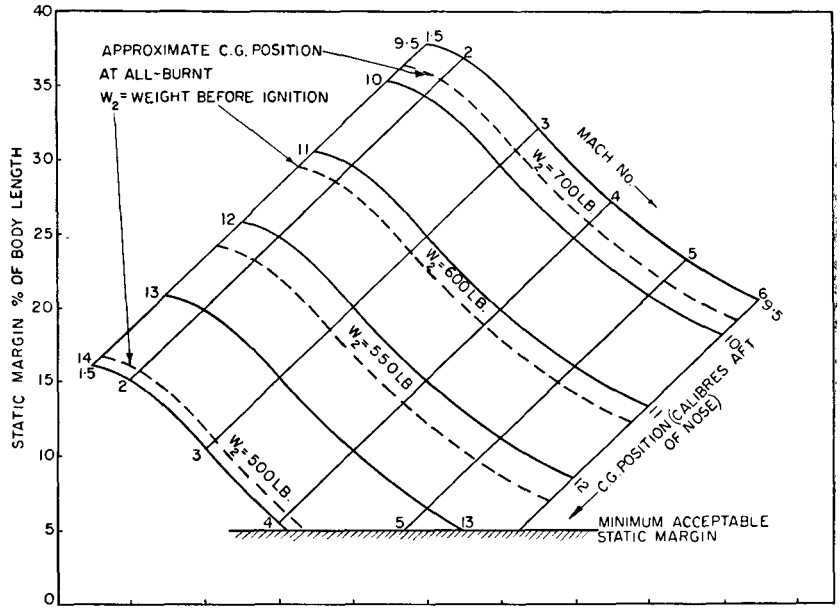

FIGURE 13. Static margin of second stage as a function of centre of gravity and Mach number.

margin below the acceptable minimum of 5 per cent of body length in the final coasting period unless the payload can be so arranged to bring the c.g. forward.

4. The Effect of Weight and Launch Elevation on Performance

The preceding discussion on design considerations applies equally to both Long Tom and Aeolus. Long Tom is considered in detail in the following paragraphs on performance; Aeolus has a lower performance, the order of the comparison being indicated by Fig. 8.

4.1. THE EFFECT OF WEIGHT AND LAUNCH ELEVATION ON PERFORMANCE FOR LONG TOM

In a typical Long Tom round of all-up weight of the order of 2,000 lb. the boost stage weighs about 1,400 lb. and the second stage 600 lb. The weight of the boost stage does not alter significantly from round to round. The weight of the second stage can vary between 520 lb. and 700 lb., depending on the instrumentation carried.

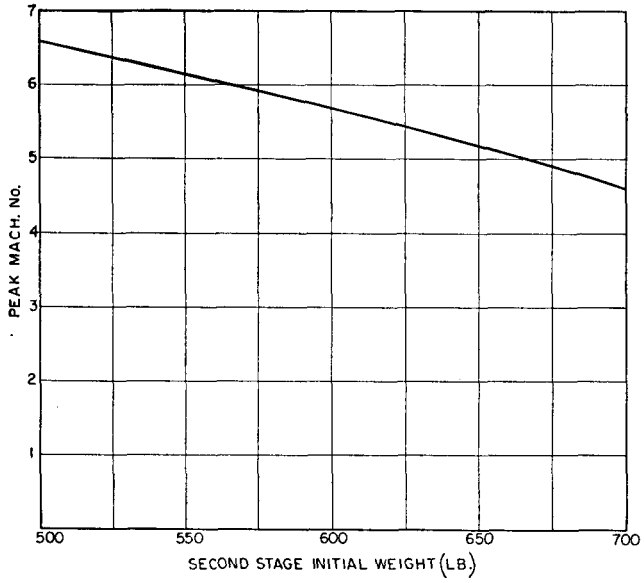

FIGURE 14. Variation of peak Mach number with second stage weight.

Thus the all-up weight of the second stage is the parameter to be considered when assessing the effect of weight on performance. In this section a constant second stage ignition time of 20 sec. and constant all-up weight of 1,400 lb. for the first stage have been assumed. In Fig. 15 peak altitude has been plotted as a function of the launch angle and initial weight of the second stage. The approximate payloads for each weight are indicated.

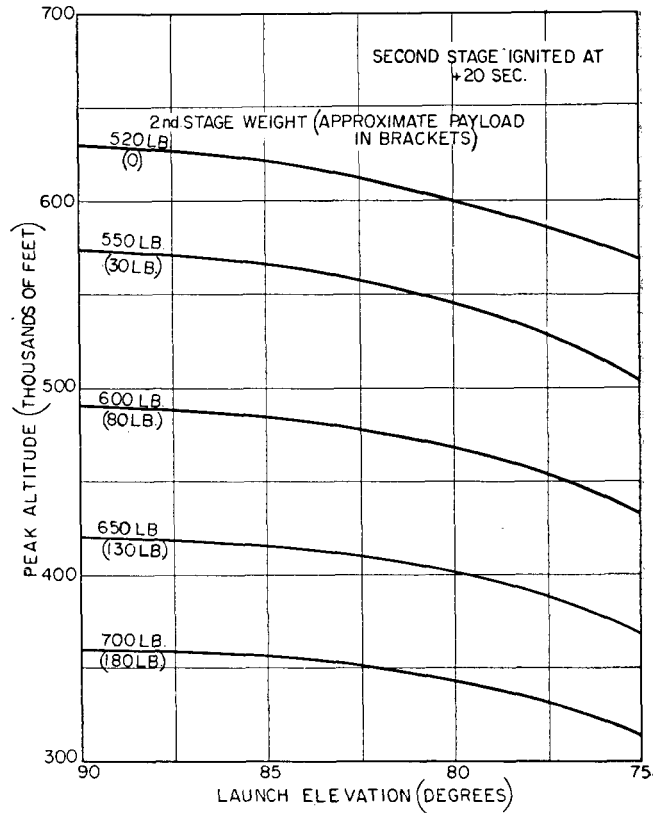

FIGURE 15. Long Tom. Peak altitude as a function of second stage weight and launch elevation.

Downloaded from https://www.cambridge.org/core. The Librarian-Seeley Historical Library, on 31 Mar 2017 at 17:38:00, subject to the Cambridge Core terms of use, available at https://www.cambridge.org/core/terms. https://doi.org/10.1017/S0368393100072667

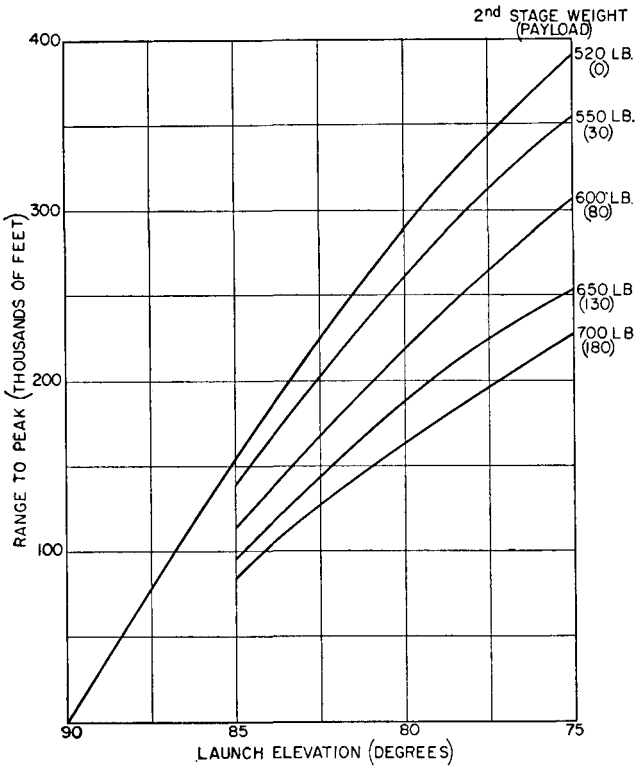

FIGURE 16. Long Tom. Range to peak altitude as a function of launch elevation and second stage weight.

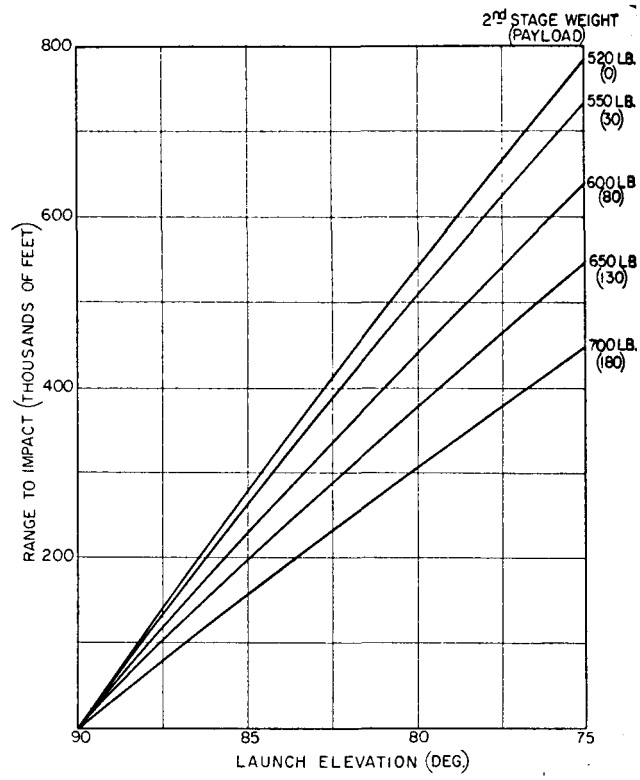

FIGURE 17. Long Tom. Range to impact as a function of launch elevation and second stage weight.

For the maximum weight considered, 700 lb., the peak altitude varies from 310,000 ft. at a launch angle of 75° to 360,000 ft. at 90°. It should be noticed that above 82·5° the increase of altitude with launch angle is small, but the peak altitude drops off more rapidly as the angle is lowered below 82·5°. The gain in altitude due to reduction in weight is substantial, being 1,600 ft. per lb. of initial second stage weight at weights below 600 lb. Between 600 lb. and 700 lb. the gain is of the order of 1,200 ft. per lb. of second stage weight.

For a typical round weighing 600 lb., altitudes of the order of 470,000 ft. could be expected. Range to peak altitude is shown in Fig. 16, while Fig. 17 shows range to impact.

As will be seen from Fig. 17 ground ranges can be considerable. A typical round with a second stage of the order of 40 miles. A drop in launcher elevation weight of 600 lb. launched at 85° covers a ground range of 5° to 80° increases the range to 80 miles. If the weight is reduced to 520 lb.—*i.e.* if the rocket is used purely as a sighter—the ground range for an 80° launch is in the region of 100 miles, while if the launcher elevation were reduced to 75° the range would increase to 150 miles.

5. Effect of Time of Ignition of Second Stage

Peak altitude as a function of second-stage ignition time and launch angle has been plotted in Fig. 18 for a second stage initial weight of 650 lb. The effect of ignition time is not very great, the altitude being increased by only some 25,000 ft. when the time of ignition is reduced from 25 sec. to 15 sec. Delaying the time of ignition beyond 25 sec. would result in an excessive decrease in performance; reducing it below 15 sec. would not result in any appreciable gain in peak altitude and would intensify the aerodynamic heating effects, due to the fact that the highest velocities are reached at lower altitudes. It has been the general practice at W.R.E. to ignite the second stage at +20 sec.

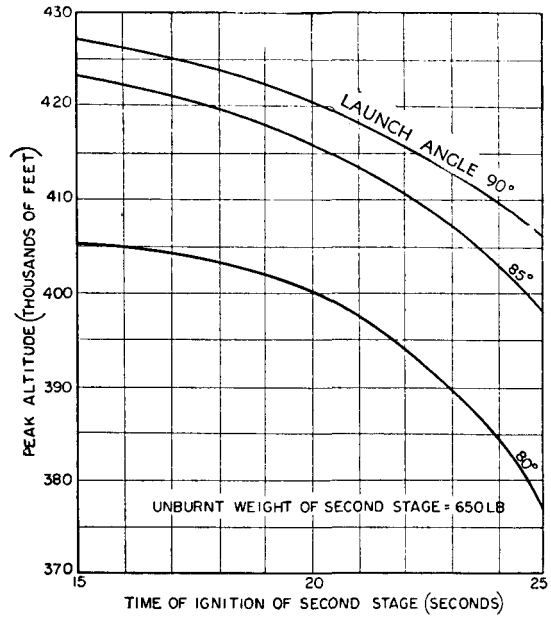

FIGURE 18. Peak altitude as a function of second-stage ignition time and launch angle.

Downloaded from https://www.cambridge.org/core. The Librarian-Seeley Historical Library, on 31 Mar 2017 at 17:38:00, subject to the Cambridge Core terms of use, available at https://www.cambridge.org/core/terms. https://doi.org/10.1017/S0368393100072667

6. Conclusions

The development of vehicles suitable for exercising and testing instrumentation at Woomera Range has resulted in the production of vehicles that are also suitable as sounding rockets for general experiments at altitudes up to about 100 miles. These two-stage vehicles (Long Tom and Aeolus), when compared with current single-stage sounding rockets of similar capabilities, have certain advantages as to ease of launching; the major disadvantage of the two-stage technique in this instance is the high longitudinal acceleration associated with short-burning, high-thrust solid fuel motors. At the end of burning of the second stage Long Tom has a peak acceleration in the region of 50*g*. However, the telemetry components, transducers, etc., that have been carried in Long Tom and Aeolus have operated adequately in this environment.

A logical development of Long Tom as a sounding rocket would be to extend the burning time of the first stage without changing the total impulse, shaping the thrust curve to keep the launch acceleration at a high value while reducing the in-flight acceleration, and hence the peak velocity and drag. This should result in a marked improvement in altitude performance. The type of thrust shaping required is quite possible with modern solid fuel motor design techniques.

ACKNOWLEDGMENTS

Acknowledgment is made by the author to the Chief Scientist, Australian Defence Scientific Service, Department of Supply, for permission to publish this paper.

REFERENCES

1. Boswell, R. W. M. (1958). Guided Flight Trials. *Journal of the Royal Aeronautical Society*, Vol. 62, No. 570, June 1958.
2. Dorling, E. B. (1959). Skylark, A High Altitude Research Rocket. *Discovery*, March 1959.
3. Kopal, Z. (1947). Tables of Supersonic Flow Around Cones. M.I.T. Technical Report 1, 1947.
4. Bishop, R. A. and Cane, E. G. (1956). Charts of the Theoretical Wave Drag of Wings at Zero-lift. R.A.E. Tech. Note Aero 2321, June 1956.
5. Monaghan, R. and Johnson, J. E. (1949). The Measurement of Heat Transfer and Skin Friction at Supersonic Speeds. Part II, R.A.E. Tech. Note. Aero 2031, December 1949.
6. Love, E. S. (1957). Base Pressure at Supersonic Speeds on Two Dimensional Airfoils and on Bodies of Revolution with and without Fins having Turbulent Boundary Layers. N.A.C.A. Tech. Note 3819, January 1957.
7. Cortright, E. M. (1956). Some Aerodynamic Considerations of Nozzle-After Body Combinations. *Aeronautical Engineering Review*, Vol. 15, No. 9, September 1956.
8. Pitts, W. C., Nielsen, J. N. and Kaattari, G. E. (1957). Lift and Centre of Pressure of Wing-Body-Tail Combinations at Subsonic, Transonic and Supersonic Speeds. N.A.C.A. Report 1307, 1957.
9. Allen, H. J. and Perkins, E. W. (1951). A Study of Effects of Viscosity on Flow over Slender Inclined Bodies of Revolution. N.A.C.A. Report 1048, 1951.
10. Buford, W. F. (1958). The Effects of After Body Length and Mach Number on the Normal Force and Centre of Pressure of Conical and Ogival Nose Bodies. *Journal of the Aeronautical Sciences*, Vol. 25, No. 2, February 1958.
11. Syvertson, C. A. and Dennis, D. H. (1957). A Second-Order Shock Expansion Method Applicable to Bodies of Revolution near Zero Lift. N.A.C.A. Report, 1328, 1957.
12. Phythian, J. E. and Dommett, R. L. (1958). Semi-empirical Methods of Estimating Forces on Bodies at Supersonic Speeds. *Journal of the Royal Aeronautical Society*, Vol. 62, No. 571, July 1958.

Downloaded from https://www.cambridge.org/core. The Librarian-Seeley Historical Library, on 31 Mar 2017 at 17:38:00, subject to the Cambridge Core terms of use, available at https://www.cambridge.org/core/terms. https://doi.org/10.1017/S0368393100072667